

Design and Optimization of an Umbrella-Type Shield Based on 3D CFD Simulation Technology

Longfei Li¹ – Xin He¹ – Taowei Jiao¹ – Yumeng Xiao¹ – Xipan Wei^{1,2} – Wei Li^{1,*}

¹ Northwest A&F University, College of Mechanical and Electronic Engineering, China

² Weichai Power Co., Ltd, China

Mechanical shields can effectively alleviate the problems of low pesticide utilization and severe environmental pollution. This manuscript uses a computational fluid dynamics (CFD) method to investigate the anti-drift mechanism of mechanical shields, study the airflow forms around them, and establish an accurate simulation model. The aerodynamic characteristics of six shields were studied, and their anti-drift effect was compared. Then, the size and working parameters were optimized using the response surface methodology (RSM). Mechanical shields can significantly improve the fog droplet deposition rate (DR) compared with the conventional spray method (no shield), among which the umbrella-type shield has the best effect; optimizing the size and selecting suitable working parameters can increase the DR to 77.31 %. The field trial showed that the DR of the conventional spray method was reduced by 31.9 % at 5 m/s compared with 3 m/s, while the DR of the shield spray method was reduced by only 3.6 % at 5 m/s compared with 3 m/s, which proved the excellent performance of the mechanical shields. The field trial results were consistent with the CFD simulation, and the relative deviation of the DR between the two was within 4 %, so the accuracy and reliability of the CFD simulation model were proved.

Keywords: mechanical shield, anti-drift, CFD simulation

Highlights

- Designed and optimized a new shield (umbrella-type shield) and conducted experimental validation.
- Put the mechanical shields into a 3D model to study them and establish an accurate simulation model.
- CFD was applied to simulate the spray flow fields of six mechanical shields to obtain their continuous phase and discrete phase information.
- Simulate the spray process deposited on the leaf surface of the target plant and compare it with the field trial results.

0 INTRODUCTION

Spraying pesticides is a powerful means of combatting plant diseases, pests, and weeds. The smaller the particles of the sprayed solution, the better the coverage and penetration of the solution [1]; spraying can improve the control effect of diseases, pests, and weeds [2]. However, the smaller the particle size of the drug solution, the weaker its ability to resist external environmental changes. This is mainly seen in poor drift resistance and a low fog droplet deposition rate (*DR*).

Mechanical shields are deflector devices installed near the nozzles of sprayers. During spray operation, the shields can change the velocity and direction of airflow around the nozzles, thus changing the trajectory of the fog droplets and deposition of coercive fog droplets to the target [3]; mechanical shields have thus demonstrated significant value in reducing droplet drift and improving pesticide utilization. While some studies examined the application of mechanical shields, research focusing on their drift reduction mechanisms and optimization remains relatively limited [4] and [5].

In previous research, Ozkan et al. [6] investigated the effectiveness of nine types of mechanical shields in reducing droplet loss using the distance from the nozzle to the droplet mass centre as an evaluation parameter in wind tunnel conditions. Although the experiments ultimately demonstrated the effective reduction of droplet drift by the shields, wind tunnel test conditions are demanding, with high costs per trial and results that may lack intuitiveness. Similarly, Tasy et al. [7] evaluated several types of mechanical shields using two-dimensional (2D) computational fluid dynamics (CFD) software and noted their good drift reduction performance when appropriate operating parameters such as spray pressure and droplet release angles were selected, but they did not delve into other factors or causes.

In contrast, this study seeks to explore the airflow patterns and aerodynamics surrounding mechanical shields in greater depth and simulate the three-dimensional (3D) dynamics of droplet drift and deposition. By employing 3D CFD simulation, we aim to investigate the drift reduction mechanisms of shields and further enhance their effectiveness, providing valuable technical insights for optimizing and improving mechanical shields. The motion of

the droplets can be considered to be a fluid motion. Methods for studying fluid motion are usually characterized by complex experiments and difficult-to-observe results; however, the emergence of CFD has broken this deadlock. CFD simulation is a method dedicated to studying fluid motion; compared to traditional wind tunnel experiments, CFD simulation offers advantages in terms of lower device complexity, cost-effectiveness, reliable variables, and experimental reproducibility, thereby presenting extensive prospects for application [8] and [9].

The primary objective of this study is to explore the drift reduction mechanisms of mechanical shields through 3D simulation models and further improve their effectiveness in reducing drift. This research aims to provide technical references for the optimization and improvement of mechanical shields. By studying the airflow models surrounding the shields and corresponding droplet trajectories, we will determine the impact of different shields on the DR and select the shield with the best performance. Additionally, we will investigate the optimal size and operating parameters of the shield to further enhance its drift reduction efficiency. Finally, we will validate the reliability of the simulation results through field experiments, thereby confirming the practical value and novelty of this research.

1 METHODS AND EXPERIMENTAL

1.1 Mechanical Shield Structure Determination

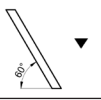
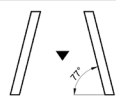
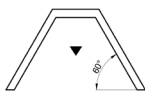
Mechanical shields can be divided into many types according to shape. In this manuscript, six types of shields were designed and selected for comparative investigation based on several mainstream shield forms. Their specific structural shapes are shown in Table 1.

1.2 Air-Liquid Two-Phase Flow Theory

The choice of using the theory of continuous phase and dispersed phase is based on the characteristics and phenomena of multiphase flow, which involves the interaction and transfer processes between two or more phases, such as the interaction between gas and liquid droplets, droplet collision, and deposition. These phenomena need to be described using appropriate physical property models to achieve accurate simulation and prediction.

In the air-liquid two-phase flow process, the FLUENT module treats the air as a continuous phase and the fog droplets as discrete phases in the

Table 1. Types of shields (triangles indicate nozzles)

Name	Type	Structure schematic	Characteristic	Application
a	Single baffle		One baffle	
b	Double baffle		Two baffles	
c	Three-sided baffle		Three sides baffles	Whole row nozzles
d	Double circular arc		Two arc baffles with different diameters	
e	U		Arc baffle	
f	Umbrella		Hemisphere, wind-assisted	Single nozzle

continuous phase [10]. This choice stems from the relative stability of air's physical properties, making it easier to model and solve using the equations of continuous media. The motion and transfer processes of air can be described using the Navier-Stokes equations, which are commonly employed in CFD simulations as fundamental fluid mechanics equations. In contrast, the droplets are the primary focus of attention because their behaviour determines the diffusion, deposition, and effectiveness of the pesticide. Therefore, it is essential to consider the mass, size, velocity, and shape of the droplets. These attributes can be described using droplet dynamics equations and other relevant models. The standard $K-\epsilon$ turbulence model was used in the numerical simulation of the air-liquid two-phase flow of the shield spray. Considering that the volume of fog droplets is tiny in proportion to the whole flow field, the momentum of fog droplets is much smaller than the momentum of the airflow. The influence of fog droplets on the airflow field is ignored and can be calculated as steady-state incompressible flow. Since the spray operation is carried out at room temperature, there is no need to consider energy transfer; only the conservation of mass and the conservation of momentum needs to be considered [11] and [12].

The conservation of mass equation is:

$$\frac{\partial p}{\partial t} + \text{div}(\rho U) = 0, \quad (1)$$

where ρ is the density of fluid [kg/m³], t time [s], div divergence, and U velocity vectors.

For steady-state incompressible flow, the velocity dispersion is zero, i.e.:

$$\text{div}(U) = \frac{\partial u}{\partial x} + \frac{\partial u}{\partial y} + \frac{\partial u}{\partial z} = 0. \quad (2)$$

The conservation of momentum equation is the Navier-Stokes equation [8], and the conservation of momentum equation of viscous incompressible fluid is:

$$\frac{\partial(u)}{\partial t} + \text{div}(uU) = S_u - \frac{1}{\rho} \frac{\partial p}{\partial x} + \text{div}(v\text{grad}u), \quad (3)$$

$$\frac{\partial(v)}{\partial t} + \text{div}(vU) = S_v - \frac{1}{\rho} \frac{\partial p}{\partial y} + \text{div}(v\text{grad}v), \quad (4)$$

$$\frac{\partial(w)}{\partial t} + \text{div}(wU) = S_w - \frac{1}{\rho} \frac{\partial p}{\partial z} + \text{div}(v\text{grad}w). \quad (5)$$

Among which:

$$\left\{ \begin{aligned} \text{grad}(u) &= \frac{\partial(u)}{\partial(x)} + \frac{\partial(u)}{\partial(y)} + \frac{\partial(u)}{\partial(z)} \\ \text{grad}(v) &= \frac{\partial(v)}{\partial(x)} + \frac{\partial(v)}{\partial(y)} + \frac{\partial(v)}{\partial(z)} \\ \text{grad}(w) &= \frac{\partial(w)}{\partial(x)} + \frac{\partial(w)}{\partial(y)} + \frac{\partial(w)}{\partial(z)} \end{aligned} \right., \quad (6)$$

$$\left\{ \begin{aligned} S_u &= Fx / \rho \\ S_v &= Fy / \rho, \\ S_w &= Fz / \rho \end{aligned} \right. \quad (7)$$

where u, v, w are the components of U in the $x, y,$ and z directions, ν kinematic viscosity [m²/s], p intensity of pressure [MPa], and S_u, S_v, S_w generalized source items.

In the process of gas-liquid two-phase flow, there is always a mutual transfer of mass and momentum between the two phases. Therefore, the control equations for the continuous phase (air) and the discrete phase (fog droplet) must be solved alternately until the solutions for both phases converge.

The momentum value and mass value transferred from the continuous phase to the discrete phase are calculated according to the change in momentum and mass [13].

The value of the change in fog droplet momentum is:

$$F = \sum \left[\frac{3\beta\mu C_D Re}{4\rho_p d_p^2} (u_p - u) + F_O \right] \cdot m_p \Delta t. \quad (8)$$

The value of the change in fog droplet mass is:

$$M = \frac{\Delta m_p}{m_{p,0}} \dot{m}_{p,0}, \quad (9)$$

where μ is viscosity of continuous phase fluid [N·s/m²], C_D drag coefficient, Re relative Reynolds number of fog droplets, ρ_p density of discrete phases [kg/m³], d_p diameter of the droplets [m], u_p discrete phase velocity [m/s], u continuous phase velocity [m/s], F_O other forces [N], \dot{m}_p mass flow rate of fog droplets [kg/s], and t time [s].

1.3 CFD Simulation Model Building

The nozzles were selected from the Lechler 110-05 standard vertebral fan nozzle produced by Lechler, Germany, whose fog droplet size distribution meets the Rosin-Rammler distribution law. The Visi Sizer DP Particle Sizing System Model 6401 (Tianjin Celes Automation Technology Co., Ltd., Tianjin, China) can measure the nozzle fog droplet spectrum, where the smallest fog droplet size of 17.5 μm, the largest particle size of 340 μm, and the medium diameter of 150.4 μm. The Rosin-Rammler distribution law assumes an exponential relationship between the fog droplet diameter and the mass fraction of fog droplets larger than this diameter.

$$Y_d = e^{-(d/\bar{d})^n}, \quad (10)$$

where Y_d is the mass percentage of fog droplets with a diameter greater than d [%], d fog droplet diameter [μm], \bar{d} average fog droplet diameter [μm], and n dispersion coefficient.

When $d = \bar{d}$, $Y_d = e^{-1} \approx 0.368$ is obtained by the interpolation method $\bar{d} = 171.7 \mu\text{m}$. The fog droplet parameters d and Y_d are arranged in the format of the Rosin-Rammler distribution, and the dispersion coefficient n is calculated and finally averaged \bar{n} .

The dispersion coefficient n is calculated as follows:

$$n = \frac{\ln(-\ln Y_d)}{\ln(d/\bar{d})}. \quad (11)$$

From Eqs. (10) and (11), the average value of the dispersion coefficient $\bar{n} = 2.762$ can be calculated.

In the FLUENT simulation, the jet source (nozzle) released 2000 fog droplets at the same velocity of 20 m/s. A simulation area is established to

simulate a wind tunnel. Referring to previous studies [14] and [15], the nozzle is set in the shield from the bottom of the simulated flow field height of 0.5 m, 1 m downwind from the natural wind inlet, and the fog droplet release angle vertically down, as shown in Fig. 1.

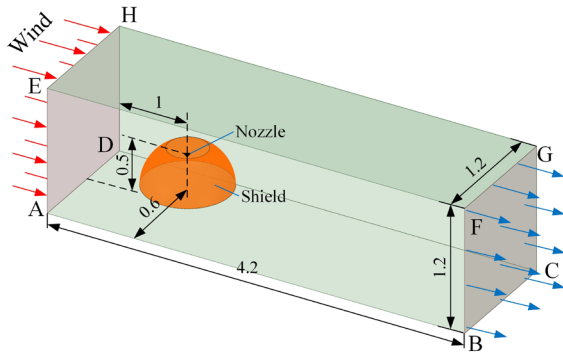


Fig. 1. Flow field simulation area, units in [m]

In the calculation area shown in Fig. 1, the ground (ABCD) is set to “trap”, and the trajectory calculation is terminated when the fog droplet moves this, and the fog droplet is deposited. The sides (ABFE, CDHG), top (EFGH), and back (BCGF) are set as the “escape” boundary. When the fog droplets move to the “escape” boundary, they are considered to have drifted, and the trajectory calculation is terminated. By setting the shield surface to “trap”, the trajectory calculation is terminated when the fog droplet reaches this interface, and the fog droplet is considered to have drifted. According to the operation specification of the plant protection machinery, the sprayer is not allowed to work when the natural wind in the field is above level 3 (3.4 m/s to 5.4 m/s), so the wind speed is set to 5 m/s.

The physical properties of the continuous and discrete phases used in the model are shown in Table 2 (the data are calculated values, except for temperature, and flow velocity, which are measured data).

Table 2. Properties of continuous and discrete phases

Continuous phase (air)		Discrete phase (fog droplet)	
Temperature [K]	293	Temperature [K]	293
Density [kg/m ³]	1.225	Density [kg/m ³]	998.2
Thermal conductivity [W/(mK)]	0.025	Thermal conductivity [W/(mK)]	0.599
Viscosity [mPa·s]	0.0176	Viscosity [mPa·s]	1.0100
Molar mass [g/mol]	28.97	Molar mass [g/mol]	18.02
Turbulence intensity [%]	20	Vaporization temperature [K]	273
Flow velocity [m/s]	5	Surface tension [N/m]	0.07275

2 RESULTS AND DISCUSSION

2.1 CFD Simulation

Due to the disjointed nature of the 3D space, the simulation results are visualized using the centre section of the model.

2.1.1 Mechanical Shields Performance Comparison

Fig. 2. shows the results of concurrent flow field simulations of continuous phase velocities for six types of shields, with colour differences to distinguish the flow velocities.

The blocking effect of the baffles (Figs. 2a, b and c) inevitably leads to a low-velocity area behind the shield. The shield (Fig. 2d) creates a high-velocity airflow directly behind the spray outlet, which may force fog droplets downward and reduce interference with fog droplet trajectories in the low-velocity region. The shield (Fig. 2e) will form a certain amount of cyclonic flow inside, preventing the tiny diameter fog droplets from leaving the shield and being deposited on the inner surface of the shield. The top and bottom of the shield (Fig. 2f) will form two high-velocity zones because of the auxiliary airflow effect, eliminating the internal vortex. In addition, the shield (Fig. 2f) can better resist the wind from all directions in the plane. In comparison, the shield (Fig. 2f) effect is more desirable.

Fig. 3. shows the trajectory of the discrete phase of the shield, with different colours representing the corresponding fog droplet diameters. It can be roughly seen that the fog droplets less than 77 µm in diameter move upward most easily.

The simulation shows that in the low velocity zone formed by the geometry of shield (Fig. 3a, b, and c) the fog droplets with smaller diameter will move in the low velocity zone and eventually drift away downwind; High velocity airflow is generated directly behind the spray outlet of the shield (Fig. 3d) forcing the smaller fog droplets downward, and only fog droplets less than 137 µm in diameter are lost from the viewing field; From the fog droplet trajectories of the shield (Fig. 3e), it can be seen that most of the fog droplets with diameters less than 77 µm cannot be detached from the inside of the shield under the action of the cyclonic flow inside the shield, and finally deposited on the shield, while fog droplets with diameters less than 166 µm will be lost from the observation field; The shield (Fig. 3f) eliminates internal cyclonic flow due to the auxiliary airflow, and the fog droplets move downward under the action

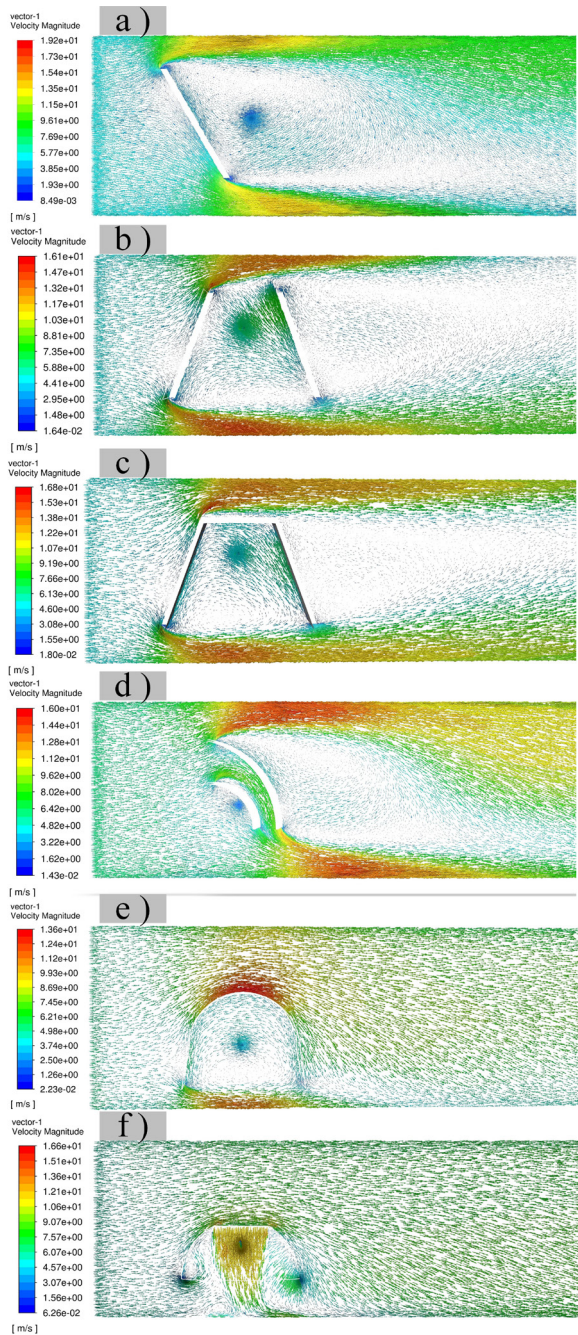


Fig. 2. Convergent flow field with continuous phase velocity

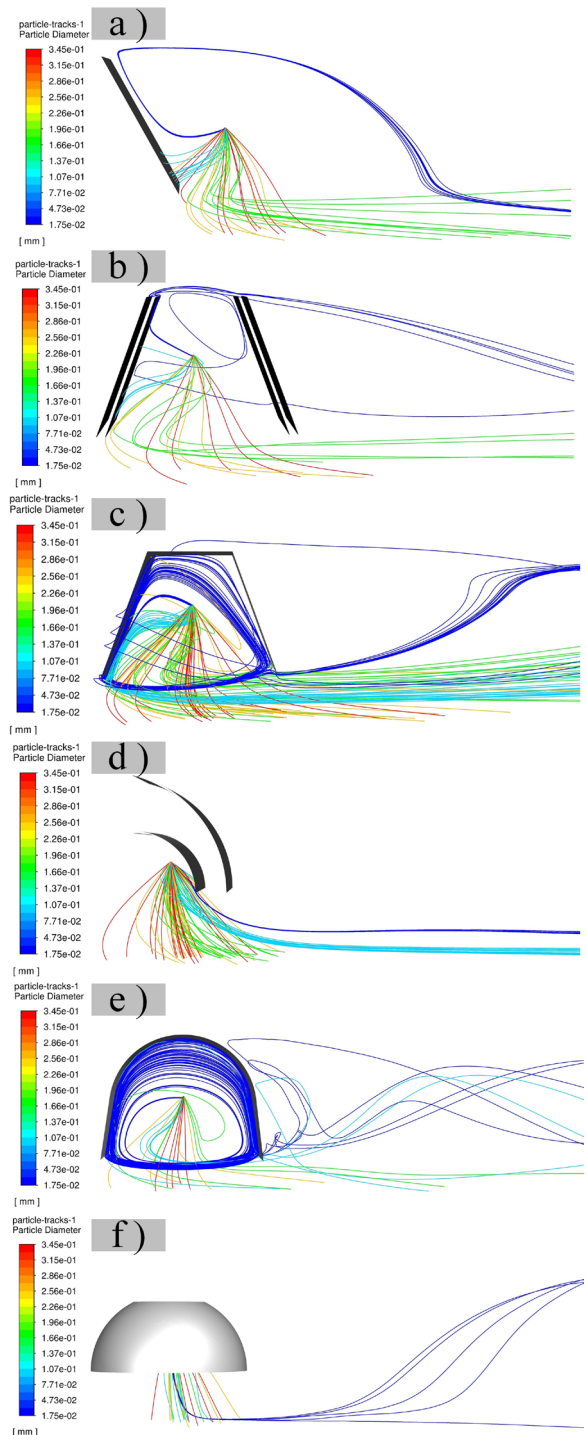


Fig. 3. Discrete phase motion trajectory of different shields

of the auxiliary airflow and are not deposited on the shield. Meanwhile, some of the fog droplets that would otherwise be lost and fog droplets larger than $77\ \mu\text{m}$ in diameter are deposited under the pushing effect of the auxiliary airflow.

The final state of the droplets can be divided into two types: deposition and loss, while droplet loss

can be divided into loss deposited on the shield and droplet drift loss, etc., where the loss deposited on the shield can be derived directly from the calculation, so the performance of several shields was evaluated by using the *DR* and the *DS* (percentage of fog droplets

deposited on the shield) as evaluation indexes. The larger the DR , the smaller the DS , and the better the anti-drift effect.

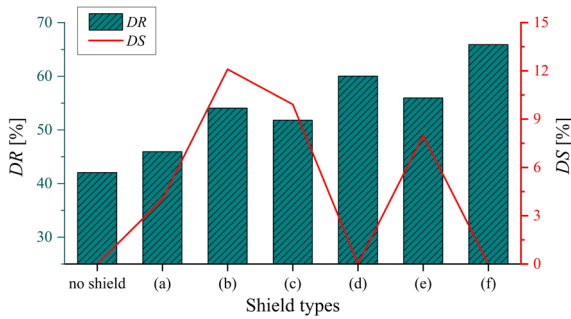


Fig. 4. Shield performance comparison

The simulation results are shown in Fig. 4, and it can be found that shield (f) (umbrella-type shield) has the highest DR and almost zero DS , so shield (f) has the best anti-drift effect among the six types of shields mentioned above.

2.2 Optimization of Shield Size and Working Parameters

The umbrella-type shield (f) structural size is shown in Fig. 5; the nozzle maximum spray angle of 110° .

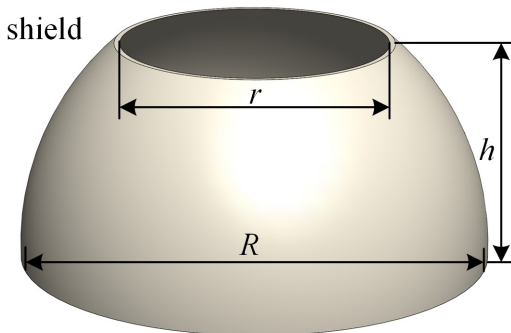


Fig. 5. Umbrella-type shield structure

2.2.1 Optimization of Shield Size Parameters

Simulation tests were conducted to improve the umbrella-type shield’s anti-drift effect for different sizes. Based on the Response Surface Methodology, the DR is used as the response value. The R (diameter of the outlet), r (diameter of auxiliary air inlet), and h (height) are used as factors, and a regression equation of response values and factors was established to obtain the optimal size parameters of the shield.

The specific factors and levels are shown in Table 3.

Table 3. Size parameters test factors and levels table

Levels	Factors		
	R [mm]	r [mm]	h [mm]
-1	400	250	200
0	500	300	240
1	600	350	280

Table 4. Simulation tests result for shield size parameters optimization

No.	Factors			DR [%]
	R [mm]	r [mm]	h [mm]	
1	500	300	240	72.62
2	400	300	200	55.46
3	400	350	240	56.44
4	500	250	280	62.63
5	500	250	200	62.75
6	600	350	240	65.45
7	500	300	240	73.87
8	500	350	280	64.46
9	600	300	200	63.64
10	500	300	240	73.11
11	400	250	240	56.63
12	600	300	280	63.21
13	500	300	240	70.21
14	500	300	240	72.53
15	400	300	280	57.88
16	600	250	240	59.89
17	500	350	200	63.17

With the help of the Box-Behnken method in Design-expert 13 software. The optimization algorithm obtained the optimal value of DR , considering multiple factors simultaneously (As Table 4).

The model’s fit $R^2 = 0.9852$ indicates that the model fits well to the DR , and the test error is small. The regression equation of the DR was imported into Origin 2022 software, and the effects of the R , r , and h on the DR were obtained, as shown in Fig. 6.

It is evident from Fig. 6 that when two of the three size parameters of the shield are fixed, the DR tends to increase and then decrease with another factor, which shows that the shield size parameters can be optimized to obtain the best value.

The nozzle’s working area can be considered a conical area with the nozzle as the vertex. Under the premise of other consistent parameters, the DR depends on the ratio X of the exit plane of the shield and the projection of the nozzle working area in the exit plane of the shield. The R , r , and h are the three primary parameters influencing the ratio X . The closer the ratio X is to the C (constant value related to the

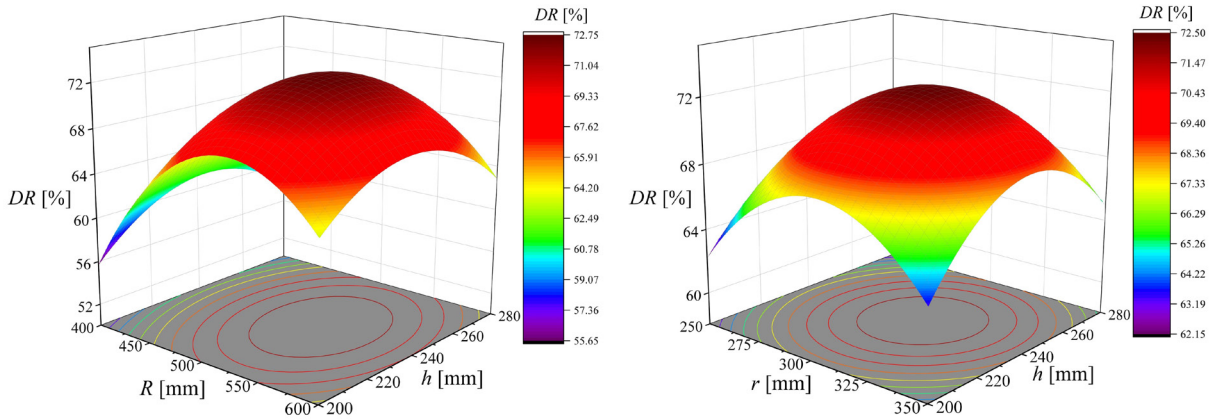


Fig. 6. Effect of shield size parameters on DR

working parameters and nozzle characteristics), the higher the DR . When the ratio X is less than C , the spray will form a high-velocity airflow in the shield, causing fog droplets to collide and be ejected, forming larger fog droplets, affecting their trajectories so that the DR decreases. In contrast, when the ratio X is bigger than C , a vortex region will be formed between the auxiliary wind and the natural wind, reducing the anti-drifting effect of the shield and the DR .

According to manufacturing accuracy and the calculation prediction of the software, when $R = 521$ mm, $r = 307$ mm, and $h = 241$ mm, the maximum DR can be 72.93 %.

2.2.2 Optimization of Working Parameters

To investigate the effect of working conditions on the anti-drift effect of the shield further [13], [16], and [17], the optimal working conditions were investigated based on the size parameters of the shield (f) obtained by optimization in the previous. The plant model is

added to the spray simulation area, consisting of dual nozzles and two parallel rows for simulation. The spray model was built, as shown in Fig. 7.

Simulation sampling and data processing are conducted by changing the blower speed N , nozzle height H (the distance between the nozzle and the shield outlet plane), and spray pressure P . The factors and levels of N , H , and P are shown in Table 5.

Table 5. Factors and levels table

Levels	Factors		
	N [rpm]	H [mm]	P [MPa]
-1	1500	100	0.3
0	2500	140	0.4
1	3500	180	0.5

With the help of Design-expert 13 software, 17 simulation tests were carried out for the design, and the optimization algorithm obtained the optimal value of DR , considering multiple factors simultaneously.

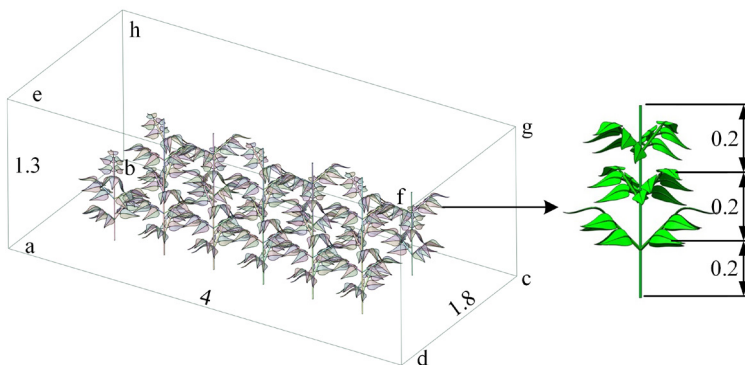


Fig. 7. Optimization model of working parameters; units in [m]

Table 6. Simulation result for working parameters

No.	Factors			DR [%]
	N [rpm]	H [mm]	P [MPa]	
1	2500	100	0.3	71.36
2	2500	140	0.4	73.67
3	3500	100	0.4	71.16
4	2500	180	0.3	76.81
5	1500	140	0.3	69.91
6	2500	140	0.4	76.56
7	2500	140	0.4	74.28
8	3500	140	0.5	67.59
9	2500	180	0.5	67.50
10	3500	140	0.3	73.82
11	1500	100	0.4	64.24
12	2500	140	0.4	73.77
13	2500	140	0.4	75.08
14	3500	180	0.4	67.90
15	1500	180	0.4	64.84
16	2500	100	0.5	69.36
17	1500	140	0.5	63.44

The simulation results (Table 6) show that the model fits well, and the possibility of test error is slight.

The regression equation and the range of values of each factor were imported into Origin 2022 software, and the effects of the N , H , and P on the fog droplet deposition rate DR were obtained, as shown in Fig. 8.

From Fig. 8, it can be seen that the rest of the factors are fixed values.

The DR increases and then decreases with increasing the N . It is because the bigger the N in a particular range, the greater the blower creates the auxiliary wind, and the more the rapid deposition of fog droplets reduces drift; however, due to the limitations of the shield structure, the auxiliary wind speed is too large to make the droplets too concentrated and difficult to spread, resulting in reduced DR .

The DR increases and then decreases with increasing the H . This is because in a particular range, with the increase of the H , the ratio X gradually close to C , and DR gradually increases; however, more than the critical value, the formation of vortex areas between the auxiliary wind and natural wind, DR decreases.

The DR decreases with increasing the P . This is because the smaller the P , the larger the fog droplet particles and the stronger the ability to resist the

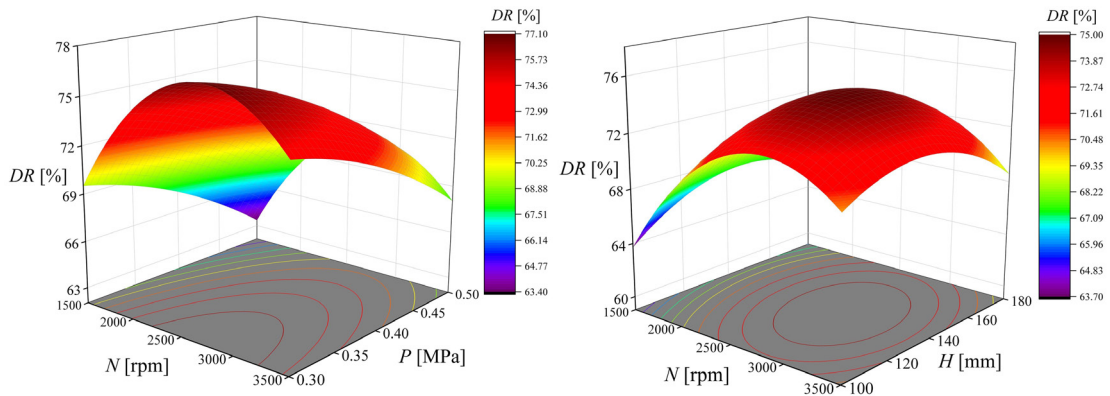


Fig. 8. Effect of each working parameter on DR

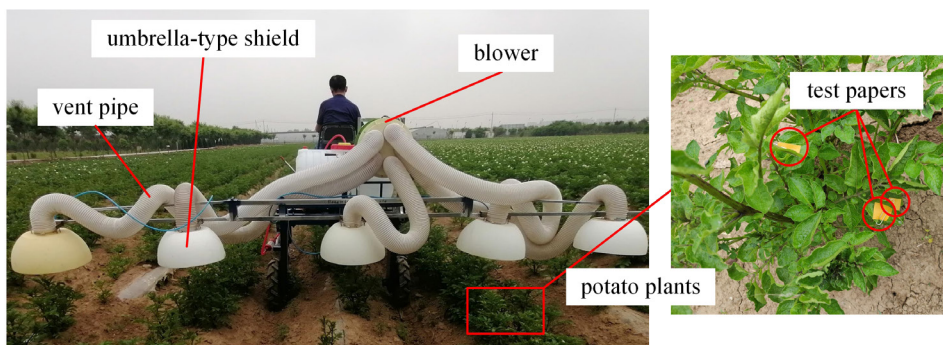


Fig. 9. Spray system structure

natural wind; however, in practice, the P must not be less than 0.3 MPa.

By combining calculation and practice, the optimum spray working conditions were found when $P = 2700$ rpm, $H = 150$ mm, $P = 0.3$ MPa, and the maximum DR can be 77.31 %.

2.3 Validation

To evaluate both the anti-drift effectiveness of the shield spray system and validate the accuracy of our CFD model, two experimental studies were conducted.

As shown in Fig. 9, the spray system used in the experiment consists of a blower, vent pipes, umbrella-type shields, nozzles, and related controllers. The nozzles of the sprayer were selected as the standard vertebral fan fog nozzle SC 110-05 produced by Lechler, Germany. The design of the umbrella-type shield was based on the specific test conditions required for the simulation tests.

For each group of experiments, 30 consecutive potato plants in the same row were selected, and sampling points were arranged at the highest point, 3/4 height, and 1/4 height of the leaves of 10 potato plants. Fog droplet test papers (30 mm × 40 mm) were used as the sampling sheets, with one sheet placed on the surface of each selected leaf. A dye (Rhodamine-B) was added to the water used as the pesticide (concentration: 0.2 %). The amount of spray liquid applied was recorded after the completion of the test and the drying of the fog droplets on the sampling sheets. Similar to the principle of water-sensitive paper, the fog droplets reacted with the dye and appeared blue.

Based on the results obtained from the fog droplet test papers, the DR was derived using Eq. (12), which is an equation specific to the analysis of the test data. Each experiment was repeated three times, and the average value was calculated to ensure the accuracy and reliability of the results.

2.3.1 Anti-Drift Effect Comparison Test

The test was designed to verify the practical effectiveness of the umbrella shield in reducing spray drift. External wind speeds were set as independent variables at 3 m/s and 5 m/s, and the rest of the parameters were kept constant: spray pressure was 0.4 MPa, blower speed was 3000 rpm, and nozzle height was 150 mm. The control group was set up with conventional spray (no shield).

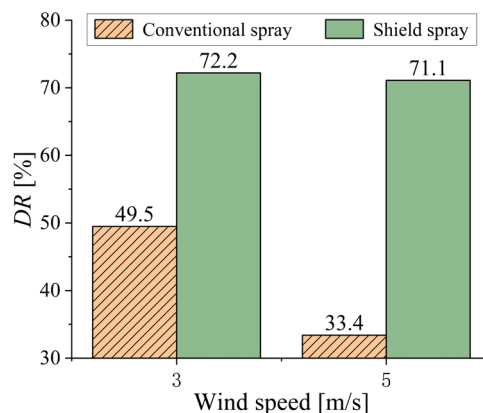


Fig. 10. Comparison of DR between the two methods

It can be seen from Fig. 10. that the DR of the shield spray method is much higher than that of the conventional spray method. The DR of the conventional spray method is greatly affected by the wind speed, and the DR decreases significantly as the wind speed increases. When the external wind speed increased from 3 m/s to 5 m/s, the DR before and after comparison during the conventional spray method decreased by 32.5 %, which was a large change, while the DR before and after comparison of the shield spray method decreased by only 1.5 % which was an insignificant change. The comparison test proved that the mechanical shield played a significant role in anti-drift during the spray process.

2.3.2 CFD Simulation Accuracy Verification Test

The simulation results were evaluated using the DR and the distribution coefficient of variation (CV) as evaluation indexes to verify the accuracy of the CFD model. The blower speed N was adjusted to 1000 rpm, 2000 rpm, and 2700 rpm, the nozzle height H was 150 mm, the spray pressure P was 0.3 MPa, and the natural wind speed was about 3.4 m/s.

(1) The fog droplet deposition rate

The test value of DR can be obtained from the ratio of the deposition volume per unit area to the spray volume per unit area in the application area [18], calculated as:

$$DR = \frac{\bar{m} \times LAI \times S_a}{m_a} \quad (12)$$

where \bar{m} is the mean value of fog droplet deposition rate per unit area of target plants, LAI leaf area index, S_a the projected area of leaves in the test area, and m_a application rate in the test area.

The results were entered in Table 7, where DR is the fog droplet deposition rate obtained from the field trial and DR_F is the fog droplet deposition rate obtained from the simulation.

Table 7. The fog droplet deposition rate

N [rpm]	DR [%]	DRF [%]	Relative deviation [%]
1000	68.25	70.83	3.78
2000	71.84	73.59	2.44
2700	74.56	77.22	3.67

(2) The distribution coefficient of variation

Numerical analysis was used to calculate the mean values of fog droplet deposition on the target plants' upper, middle, and lower foliage to calculate the CV , which indicates the deviation of fog droplet deposition on each leaf layer of the target plant from the mean value; the smaller the value, the better the uniformity of fog droplet deposition distribution [19].

$$CV = \left(\sqrt{\frac{\sum_{i=1}^n (q_i - \bar{q})^2}{n-1}} / \bar{q} \right) \times 100 \%, \quad (13)$$

where q_i is fog droplet deposition for the i^{th} sample [$\mu\text{g}/\text{cm}^2$], \bar{q} is the average value of fog droplet deposition [$\mu\text{g}/\text{cm}^2$], and n is total number of samples.

Table 8. Coefficient of variation of the distribution of fog droplet deposition

N [rpm]	CV [%]	CVF [%]	Relative deviation [%]
1000	18.59	17.34	6.72
2000	20.32	18.98	5.59
2700	13.58	12.76	6.01

The calculated results are shown in Table 8, where CV is the coefficient of variation of the fog droplet deposition distribution from the field trial, and CV_F is the coefficient of variation of the fog droplet deposition distribution from the simulation.

It can be seen from the comparison results that the field trial results are consistent with the CFD simulation test results, with only minor deviations. The DR of the field trial is slightly smaller than the CFD simulation, and the relative deviation is within 4 %. The CV of the field trial is slightly larger than the CFD simulation, and the relative deviation is within 7 %. The main reason for the discrepancy is uncontrollable factors, such as the natural wind variation and the bounce phenomenon of fog droplets. That is what causes the loss of a small amount of fog droplets.

The field trial proved that the deviation between the CFD simulation and the actual is small and negligible, and the accuracy of the CFD model can fully meet the requirements of practical use.

3 CONCLUSIONS

The 3D CFD simulation model is more in line with the field reality (fog droplets can move in three dimensions), which is an economical and practical method for performance evaluation, especially for shield design and optimization.

1. A new type of shield has been designed. By comparing six types of shields, it was found that the umbrella-type shield has the best performance.
2. Dimensions of the umbrella-type shield have been optimized according to agronomic requirements. When $R = 521$ mm, $r = 307$ mm, and $h = 241$ mm, the maximum DR can be 72.93 %.
3. Optimal working parameters were selected according to the field operating conditions. The optimum parameters were found when $P = 2700$ rpm, $H = 150$ mm, $P = 0.3$ MPa, and the maximum DR can be 77.31 %.

Future research on mechanical shields should consider the effect of multiple nozzles working simultaneously on the simulation results and needs further study to be verified.

4 ACKNOWLEDGEMENTS

This research was funded by the Science and Technology Project of China Tobacco Corporation Shaanxi Province, Construction of a Standard System for Suitable Mechanized Tobacco Agriculture in Shaanxi Tobacco Area and Demonstration and Promotion of Integration of Agricultural Machinery (KJ-2022-02) and Agriculture and the Key Industry Chain Innovation Project of the Shaanxi Province (2018ZDCXL-NY-03-06).

5 REFERENCES

- [1] Bourdimos, G., Koutsiaras, M., Psiroukis, V., Balafoutis, A., Fountas, S. (2019). Development and field evaluation of a spray drift risk assessment tool for vineyard spraying application. *Agriculture*, vol. 9, no. 8, DOI:10.3390/agriculture9080181.
- [2] Miranda-Fuentes, A., Marucco, P., Gonzalez-Sanchez, E.J., Gil, E., Grella, M., Balsari, P. (2018). Developing strategies to reduce spray drift in pneumatic spraying in vineyards: Assessment of the parameters affecting droplet size in pneumatic spraying. *Science of the Total Environment*, vol. 616-617, p. 805-815, DOI:10.1016/j.scitotenv.2017.10.242.

- [3] Osuch, A., Przygodzinski, P., Rybacki, P., Osuch, E., Kowalik, I., Piechnik, L., Przygodzinski, A., Herkowiak, M. (2020). Analysis of the effectiveness of shielded band spraying in weed control in field crops. *Agronomy*, vol. 10, no. 4, DOI:10.3390/agronomy10040475.
- [4] Perkins, D.B., Abi-Akar, F., Goodwin, G., Brain, R.A. (2022). Characterization of field-scale spray drift deposition and non-target plant biological sensitivity: A corn herbicide (mesotrione/s-metolochlor) case study. *Pest Management Science*, vol. 78, no. 7, p. 3193-3206, DOI:10.1002/ps.6950.
- [5] Duga, A.T., Delele, M.A., Ruysen, K., Dekeyser, D., Nuyttens, D., Bylemans, D., Nicolai, B.M., Verboven, P. (2017). Development and validation of a 3D CFD model of drift and its application to air-assisted orchard sprayers. *Biosystems Engineering*, vol. 154, p. 62-75, DOI:10.1016/j.biosystemseng.2016.10.010.
- [6] Ozkan, H.E., Miralles, A., Sinfort, C., Zhu, H., Fox, R.D. (1997). Shields to reduce spray drift. *Journal of Agricultural Engineering Research*, vol. 67, no. 4, p. 311-322, DOI:10.1006/jaer.1997.0174.
- [7] Tsay, J., Ozkan, H.E., Fox, R.D., Brazee, R.D. (2002). CFD simulation of mechanical spray shields. *Transactions of the ASAE*, vol. 45, no. 5, p. 1271-1280, DOI:10.13031/2013.11055.
- [8] Hong, S.-W., Zhao, L., Zhu, H. (2018). CFD simulation of airflow inside tree canopies discharged from air-assisted sprayers. *Computers and Electronics in Agriculture*, vol. 149, p. 121-132, DOI:10.1016/j.compag.2017.07.011.
- [9] Ellis, M.C.B., Lane, A.G., O'Sullivan, C.M., Jones, S. (2021). Wind tunnel investigation of the ability of drift-reducing nozzles to provide mitigation measures for bystander exposure to pesticides. *Biosystems Engineering*, vol. 202, p. 152-164, DOI:10.1016/j.biosystemseng.2020.12.008.
- [10] Li, H., Wang, J., Wang, P., Liu, J., Yuan, X., Han, H. (2022). Effect of the installation angle of nozzle on the atomizing performance of air-assisted spraying dust suppression device. *Atmosphere*, vol. 13, no. 4, DOI:10.3390/atmos13040520.
- [11] Han, H., Wang, P., Liu, R., Tian, C. (2020). Experimental study on atomization characteristics and dust-reduction performance of four common types of pressure nozzles in underground coal mines. *International Journal of Coal Science & Technology*, vol. 7, no. 3, p. 581-596, DOI:10.1007/s40789-020-00329-w.
- [12] Wang, P., Shi, Y., Zhang, L., Li, Y. (2019). Effect of structural parameters on atomization characteristics and dust reduction performance of internal-mixing air-assisted atomizer nozzle. *Process Safety and Environmental Protection*, vol. 128, p. 316-328, DOI:10.1016/j.psep.2019.06.014.
- [13] Brown, R.B., Sidahmed, M.M. (2001). Simulation of spray dispersal and deposition from a forestry airblast sprayer - part II: Droplet trajectory model. *Transactions of the ASAE*, vol. 44, no. 1, p. 11-17, DOI:10.13031/2013.2298.
- [14] Sakakibara, N., Manabe, Y., Hiromoto, Y., Kobayashi, Y. (2008). Development of high quality thermal spraying process by shielding control. *Science and Technology of Welding and Joining*, vol. 13, no. 4, p. 344-348, DOI:10.1179/174329307x236887.
- [15] Hong, S.-W., Zhao, L., Zhu, H. (2018). CFD simulation of pesticide spray from air-assisted sprayers in an apple orchard: Tree deposition and off-target losses. *Atmospheric Environment*, vol. 175, p. 109-119, DOI:10.1016/j.atmosenv.2017.12.001.
- [16] Bonds, J.A.S., Leggett, M. (2015). A literature review of downwind drift from airblast sprayers: Development of standard methodologies and a drift database. *Transactions of the ASABE*, vol. 58, no. 6, p. 1471-1477, DOI:10.13031/trans.58.11057.
- [17] Salcedo, R., Vallet, A., Granell, R., Garcera, C., Molto, E., Chueca, P. (2017). Eulerian-Lagrangian model of the behaviour of droplets produced by an air-assisted sprayer in a citrus orchard. *Biosystems Engineering*, vol. 154, p. 76-91, DOI:10.1016/j.biosystemseng.2016.09.001.
- [18] Lv, X., Fu, X., Song, J., He, X. (2011). Influence of spray operating parameters on spray drift. *Transactions of the CSAM*, vol. 42, no. 1, p. 59-63, DOI:10.3969/j.issn.1000-1298. (in Chinese)
- [19] Wang, C., He, X., Zeng, A., Andreas, H., Supakorn, W., Qiao, B. (2020). Measuring method and experiment on spray drift of chemicals applied by uav sprayer based on an artificial orchard test bench. *Transactions of the CSAE*, vol. 36, no. 13, p. 56-66, DOI:10.11975/j.issn.1002-6819.2020.13.007. (In Chinese)